ChemComm

Accepted Manuscript

This article can be cited before page numbers have been issued, to do this please use: Q. Cao, J. Yang, H. zhang, L. Hao, G. Yang, L. Ji and Z. Mao, *Chem. Commun.*, 2019, DOI: 10.1039/C9CC03480C.

View Article Online
DOI: 10.1039/C9CC03480C

COMMUNICATION

Traceable In-cell Synthesis and Cytoplasm-to-Nucleus Translocation of A Schiff base Zinc Complex as A Simple and Economical Anticancer Strategy

Received 00th January 20xx,
Accepted 00th January 20xx

DOI: 10.1039/x0xx00000x

www. rsc.org/

Qian Cao [a]†, Jing Yang [a]†*, Hang Zhang [a], Liang Hao [a], Gang-Gang Yang [a], Liang-Nian Ji [a], and Zong-Wan Mao [a]*

We have proposed a facile and cheap cancer therapeutic strategy by in-cell synthesizing theranostic Zn Schiff base complexes with nuclear targeting and DNA damaging capability. The in-cell synthesis can be traced *via* green-to-blue fluorescence shift, and the subsequent cytoplasm-to-nucleus translocation realizes cancer-specific therapy both *in vitro* and *in vivo*.

Zinc(II) is the second most abundant transition metal in human body, and zinc homeostasis alternations have been linked to many disease.[1] Nowadays, zinc complexes have attracted a lot of interest in the field of cancer therapy based on the fact that 1) zinc(II) is significantly non-toxic even at higher doses compared with other metals (Fe, Cu, Hg, ect), which is beneficial to biocompatibility;[2-4] 2) owing to the ability in assisting Lewis activation, nucleophile generation, and rapid ligand exchange, zinc complexes can be adept in the catalysis of hydrolytic reactions, such as DNA hydrolysis and cleavage, thus making the anti-cancer activity possible.[5-6] Although many Zn complexes have been developed in this purpose and some of them exhibit excellent DNA (duplex or quadraplex) binding affinities *in vitro*,[7] their anti-cancer efficacy at cellular level are very limited and the mechanisms of action are still not very clear. This is because most of these complexes localize in the cytoplasm rather than the nucleus, resulting in negligible inhibitory activity towards DNA expression in living cells.[8] There are also a few examples of nuclear penetrated zinc complexes, such as a nitro-substituted ZnSalen reported by Laura,[9] a Zn-terpyridine complex reported by Tian,[10] and a Zn-naphthalimide complex reported by Guo,[11] however, their cytotoxicity is still very low. To the best of our knowledge, nuclear-targeted anti-cancer zinc complexes are very rare and the *in vivo* anticancer investigations are still lacking.

On the other hand, luminescent zinc complexes have been widely explored as cellular imaging agents, in which Zn(II) can stabilize the structure of the organic ligand and improve the rigidity, thus exhibiting enhanced photo-stability and quantum yield.[12-18] This also includes Zn Schiff base complexes. Moreover, some transition metal Schiff base complexes have been reported possessing unique medicinal activities *ca.* anti-bacteria, anti-tumor and anti-virus.[19-20] Inspired by these, rational design of theranostic nuclear-targeted Zn Schiff base complexes is very promising, which can simultaneously induce and monitor the therapeutic effects, thus giving insights into the anticancer mechanisms. However, such zinc complexes have not yet been reported.

In this work, we have proposed a facile and cheap cancer therapeutic strategy, in which a dated Schiff base (**L_1**) is turned into a promising theranostic agent by simply using zinc salt as an auxiliary reagent to generate a Zn-Schiff base complex (**$ZnHL_1$**) in living cells, exhibiting nuclear permeability, DNA damage capability and anti-cancer activity. As shown in **Scheme 1**, the in-cell synthesis of **$ZnHL_1$** can be traced in real-time through the Zn^{2+} induced green-to-blue fluorescence changes and cytoplasm-to-nucleus translocation. The disulfide linked Schiff base **L_1**, positively charged **$ZnHL_1$** and neutral **ZnL_1** complex were synthesized and characterized by ESI-MS, ^1H NMR, and elemental analysis (Fig. S1-S4, ESI†). **$ZnHL_1$** is found insoluble in most solvents (water, methanol, ethanol, diethyl ether) and only partly soluble in DMF and DMSO, which may seriously restrict its biological application. The solubility of neutral complex **ZnL_1** was even worse.

Initially, the selectivity of **L_1** towards a series of different biologically relevant metal ions such as Na^+, K^+, Ag^+, Ca^{2+}, Mg^{2+}, Fe^{2+},Fe^{3+}, Co^{2+}, Ni^{2+}, Cu^{2+}, Mn^{2+}, Cd^{2+}, Al^{3+}, Cr^{3+} was studied. UV-Vis spectra show that introduction of Zn^{2+} into the solution of **L_1** induces an intensive new absorption centered at 365 nm, which is not prominent in other metal ion cases (Fig. S5A, ESI†). Under 365 nm excitation, **L_1** exhibits weak green fluorescence in a DMSO-H_2O (1:1, v/v) solvent; upon introducing various metal ions (3 equiv), Zn^{2+} is the only one that induces a green-to-blue fluorescence change, while other metal ions only induce negligible fluorescence enhancement (< 10%) or

a. MOE Key Laboratory of Bioinorganic and Synthetic Chemistry, School of Chemistry, Sun Yat-Sen University, Guangzhou 510275 (P. R. China). E-mail: yangjing8@mail.sysu.edu.cn (J. Yang); cesmzw@mail.sysu.edu.cn (Z.-W. Mao).
†These authors contributed equally to this work.
Electronic Supplementary Information (ESI) available: [characterization of ligand and Zn complexes; metal ion selectivity experiment; ATP assay; changes in the nuclear morphology of apoptotic cells; and so on]. See DOI: 10.1039/x0xx00000x

View Article Online
DOI: 10.1039/C9CC03480C

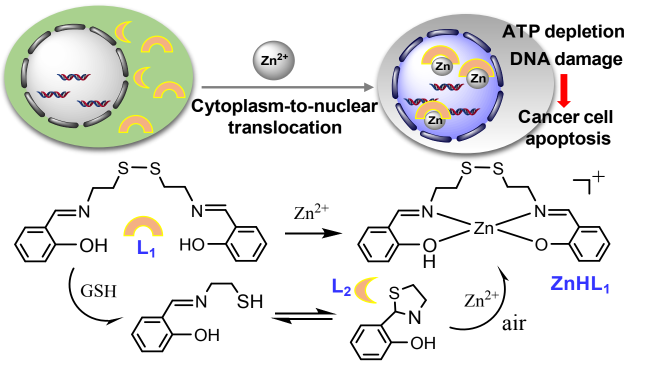

quench the emission (**Fig. 1A** and S5B, ESI †). Competition experiment was also conducted by adding more equivalents of other metal ions, showing that most of them do not interfere

Scheme 1 Zn^{2+} induced intracellular synthesis of Zn-Schiff base complex, indicated by the green-to-blue fluorescence changes followed by the cytoplasm-to-nucleus translocation, resulting in ATP depletion, nuclear DNA damage and cancer cell apoptosis.

with the fluorescence analysis of Zn^{2+} significantly (Fig. S5C, ESI†). Although excess Al^{3+}, Fe^{3+} and Cu^{2+} quench the fluorescence, these free metal ions are trace in cells which will not affect the cellular probing of abundant exogenous Zn^{2+}. These results suggest the specific fluorescence response of $\mathbf{L_1}$ to Zn^{2+}, which is visible to naked eyes.

Secondly, Zn^{2+} titration experiments were conducted in DMSO-H_2O (1:1, v/v) solvent. UV-Vis absorption spectrum of $\mathbf{L_1}$ shows a gradual decrease at 315 and 410 nm with the concomitant formation of a new band at 365 nm upon Zn^{2+} addition (**Fig. 1B**). Simultaneously, weak fluorescence of $\mathbf{L_1}$ is gradually enhanced and the emissive maxima is gradually blue-shifted from 515 nm to 455 nm (**Fig. 1C**), in which the intensity ratio of the blue and green fluorescence (I_{455}/I_{565}) displays a good linear relationship with the zinc ion concentrations in the 0-20 μM range (Fig. S6A, ESI†).The complexation stoichiometry and binding affinity of $\mathbf{L_1}$ with Zn^{2+} is found to be 1:1 by Job-plot (**Fig. 1D**) and 0.93×10^4 M^{-1} by absorption methods using Benesi-Hildebrand equation, respectively (Fig. S6B, ESI†). Moreover, upon Zn^{2+} addition the molecular ion peak of $\mathbf{L_1}$ (m/z = 361.00) disappears with the concomitant formation of a cluster peak centered at m/z = 442.60, which has been assigned to [$\mathbf{ZnHL_1}$ + H2O]$^+$ (Fig. S7A, ESI†), and the NMR signal of phenolic OH of $\mathbf{L_1}$ (13.3 ppm) gradually decreases (Fig. S7B, ESI†). These results validate the formation of $\mathbf{ZnHL_1}$ complex.

Thirdly, although $\mathbf{L_1}$ exhibits good stability at physiological pH at least in 24 h (Fig. S8, ESI †), it may easily undergo S-S bond reduction in the presence of SH containing species. ^{1}H NMR spectra show that after reacting with ehyl thioglycolate the signals of $\mathbf{L_1}$ are significantly reduced accompanied with new signals rising, for example, the O-Ha and C-Hb peaks of $\mathbf{L_1}$ at 13.30 and 8.59 ppm disappear accompanied with new O-Ha' and C-Hb' peaks emerging at 9.92 and 5.65 ppm, indicating the S-S reduction (Fig. S9A, ESI †). This is also confirmed by fluorescence spectroscopy (Fig. S9B, ESI †), in which green fluorescence from $\mathbf{L_1}$ is completely quenched after incubating with GSH (5 mM) for 10 min. However, after addition of Zn^{2+}

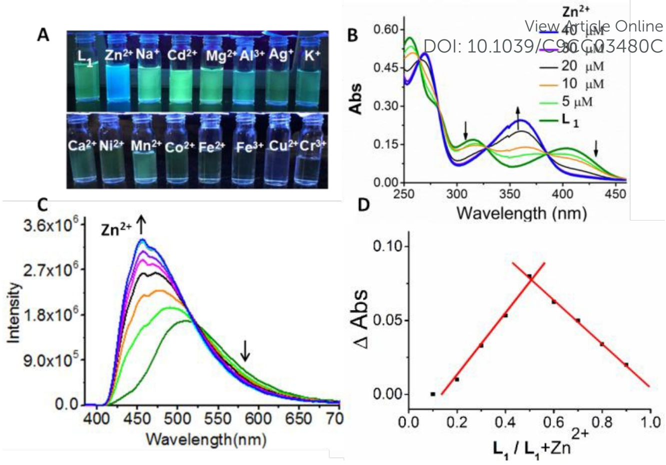

the blue fluorescence is gradually emerging and the final spectrum is similar to that of $\mathbf{ZnHL_1}$. This cascade "on-off-on" phenomenon suggests that even if GSH can cleave the S-S

Fig. 1 (A) Photographs of $\mathbf{L_1}$ in the presence of different metal ions (3 equiv) under 365 nm UV lamp; (B) UV/Vis absorption and (C) fluorescence changes of $\mathbf{L_1}$ (30 μM) with increasing concentrations of Zn^{2+} ions (0-40 μM) in DMSO-H_2O (1:1, v/v) solutions; (D) Job-plot indicates the 1:1 binding stoichiometry between $\mathbf{L^1}$ and Zn^{2+} by absorption changes at 405 nm.

bond of $\mathbf{L_1}$ to generate non-emissive $\mathbf{L_2}$, oxidative interconversion of $\mathbf{L_2}$ can take place in the presence of Zn^{2+} to still give $\mathbf{ZnHL_1}$ as the final product. The oxidative interconversion has also been proved by FTIR in previous literature.[21]

All the above results provide sufficient evidence proving the facile formation of $\mathbf{ZnHL_1}$ by simple mixing Zn^{2+} and $\mathbf{L_1}$ in solvent, and the green-to-blue fluorescence change can be used as an indicator for the intracellular formation of $\mathbf{ZnHL_1}$, no matter Schiff base undergoes S-S bond cleavage or not. Accordingly, in-cell synthesis of $\mathbf{ZnHL_1}$ is highly probable and can be traced by confocal microscopy (λ_{ex}= 405 nm). Initially, living A549 cells was incubated with $\mathbf{L_1}$ (40 μM) at 37°C for 6 h to make sure the sufficient cellular uptake of the ligand. After refreshing the culture medium, cells were further incubated with Zn^{2+} (100 μM) and cellular fluorescence at different time period was analyzed with a dual-emission mode (λ_{em}: green channel 520±20 nm; blue channel 450±20 nm). As shown in **Fig. 2A**, $\mathbf{L_1}$ displays green fluorescence mainly localizing in cytoplasm. Upon Zn^{2+} addition (0.5 h), a significant increase in the blue fluorescence is observed accompanied with a dramatic drop of the green fluorescence, indicating the in-cell formation of $\mathbf{ZnHL_1}$, which mainly localizes in cytoplasm at early stage. Co-localization experiment indicates that the blue fluorescence from $\mathbf{ZnHL_1}$ is not colocalized with mitochondria- or lysosome-specific dyes (Fig. S10, ESI †). With prolonged incubation time (up to 12 h), most of the blue fluorescence migrates from cytoplasm into nucleus, finally exhibiting a high degree of co-localization (pearson's correlation coefficient 0.80) with the commercial DNA stain Syto59 (**Fig. 2B**). This indicates the excellent nucleus penetrating ability of the in-cell synthesized $\mathbf{ZnHL_1}$. Average F_{blue}/F_{green} ratios measured from five cells in Fig. 2A shows a gradual increase with incubation time (Fig. S11, ESI†). According to ctDNA titration and EB competition experiments (Fig. S12, ESI†), **ZnHL$_1$** may interact with DNA after translocating to the nucleus, which is similar to other ZnSalen complexes.[7,13] The in-cell synthesis and distribution of **ZnHL$_1$** complex was also demonstrated by ICP-MS, in which A549 cells were incubated with different concentrations of **L$_1$** (0, 20 and 40 μM) for 12 h and then treated with the same amount of Zn^{2+} (100 μM) for another 12 h. As shown in Fig. S13 (ESI†), Zn(II) contents in the whole cell and nucleus both increase in a **L$_1$** dose-dependent manner, indicating the intracellular generation of various concentrations of **ZnHL$_1$**, *ca.* 60% of which is localized in nucleus. All these results demonstrate the efficient nuclear internalization of in-cell synthesized **ZnHL$_1$**, as indicated by the green-to-blue fluorescence change and subsequent cytoplasm-to-nucleus fluorescence translocation.

Then the *in vitro* cytotoxicity against several different cancerous (A549, HeLa, MCF-7) and normal (HLF) cell lines was determined by 48 h MTT assay. As shown in **Table 1**, treatment with either zinc salt or **L$_1$** alone does not affect the cell viability even at 100 μM. Pre-prepared **ZnHL$_1$** solution exhibits a medium cytotoxicity against cancer cells with IC_{50} values of 40~90 μM. Interestingly, when the cells are pre-treated with Zn^{2+} (100 μM, 2 h) and then incubated with various concentrations of **L$_1$** for another 46 h incubation, significantly enhanced cytotoxicity against cancer cell lines is observed with IC_{50} values of 15-20 μM, which are similar to that of cisplatin. By contrast, its cytotoxicity against normal cell line HLF is much lower with IC_{50} values of *ca.* 95~98 μM, suggesting the capability of **ZnHL$_1$** to selectively kill cancer cells. This may be due to the relatively higher accumulation of **ZnHL$_1$** in cancer cells (Fig. S14, ESI†).

Furthermore, the anticancer mechanism of in-cell synthesized **ZnHL$_1$** was investigated (**Fig. 3**). Firstly, Annexin V/PI double staining experiment shows that the capability of

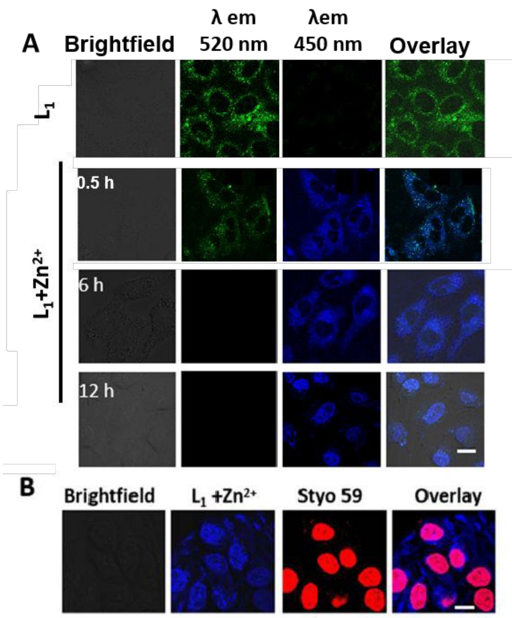

Fig. 2 (A) Confocal images of A549 cells incubated with **L$_1$** (40 μM, 6 h) followed with $ZnCl_2$ treatment (100 μM, up to 12 h), λ_{ex} = 405 nm; (B) Colocalization of intracellular synthesized **ZnHL$_1$** (40 μM, 12 h) with nuclear dye Styo-red ($\lambda_{ex}/\lambda_{em}$ = 622/645 ± 20 nm) in A549 cells. Scale bar: 5 μm.

Table 1 IC_{50} (μM) values of tested compounds towards different cell lines.

Compound	A549	MCF-7	HeLa	HLF
L$_1$	>100	>100	>100	>100
$ZnCl_2$	>100	>100	>100	>100
ZnHL$_1$	50.3 ±4.5	41.2 ±2.7	87.4 ±6.7	97.5 ±3.4
$ZnCl_2$ + **L$_1$**	21.5 ±2.1	19.3 ±2.5	16.3 ±1.9	95.5 ±7.8
Cisplatin	22.3 ±2.1	24.2 ±1.7	15.5 ±1.2	27.5 ±2.3

Zn^{2+} (100 μM, 36 h) or **L$_1$** (100 μM, 36 h) alone to induce apoptosis is negligible; however, a dramatically dose-dependent increase in the percentage of apoptotic cells is observed from 24.5 ± 0.5 % (10 μM) to 61.4 ±0.82 % (40 μM) based on the in-cell synthesis of different amount of **ZnHL$_1$** (**Fig. 3A**). Moreover, owing to the nuclear penetrating and staining ability, in-cell synthesized **ZnHL$_1$** can induce cell apoptosis and track nuclear condensation and fragmentation simultaneously (Fig. S15, ESI†).

Secondly, in-cell synthesized **ZnHL$_1$** induces a substantial decrease in the intracellular ATP levels in dose-dependent manner (25-100 μM), whereas free ligand **L$_1$** or zinc salt did not affect the ATP levels even at a high concentration of 100 μM

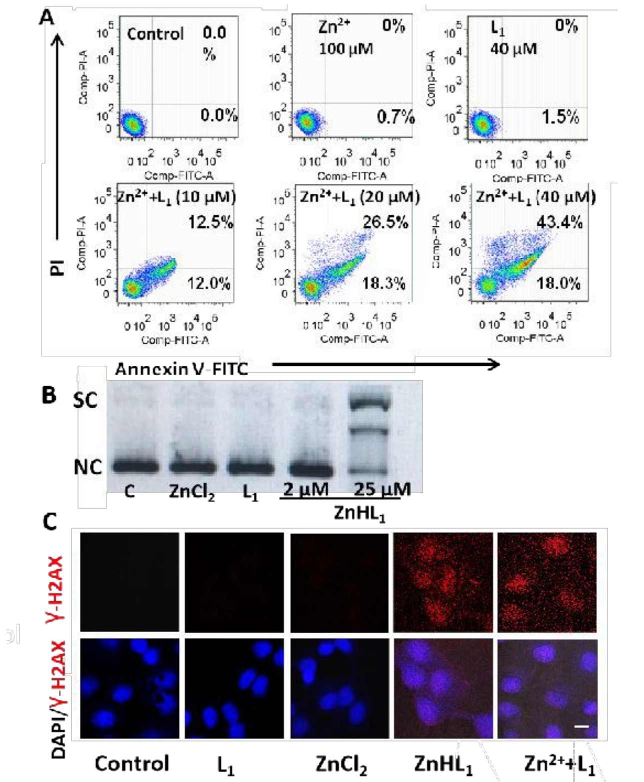

(Fig. 16, ESI†).

Fig. 3(A) Annexin V/PI assay of A549 cells treated with $ZnCl_2$, **L$_1$**, Zn^{2+}+ **L$_1$** at the indicated concentrations for 36 h. (B) Gel electrophoresis showing the cleavage of pUC19 DNA (0.5 lg); (C) Immunofluorescence of γH2AX (DNA breaks foci) in A549 cells

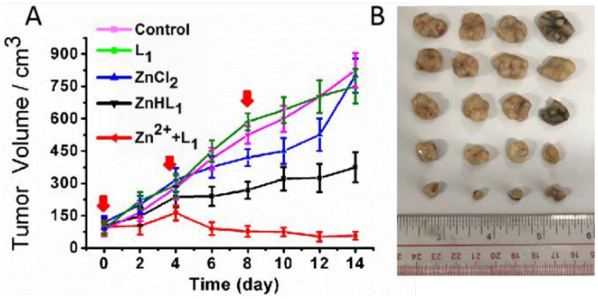

treated with various compounds for a total incubation time of 36 h. $ZnCl_2$: 100 μM, $\mathbf{L_1}$:100 μM; $\mathbf{ZnHL_1}$: 40 μM; In-cell synthesized $\mathbf{ZnHL_1}$ ($ZnCl_2$ + $\mathbf{L_1}$): 40 μM. DAPI: $\lambda_{ex}/\lambda_{em}$ =405/461 ± 20 nm; γH2AX antibody: Daylight 549. Scale bar: 5 μm.

Fig. 4 *In vivo* anti-tumor efficacy of PBS (control), $\mathbf{L_1}$, $ZnCl_2$, as-prepared $\mathbf{ZnHL_1}$ and in-cell synthesized $\mathbf{ZnHL_1}$ (Zn^{2+}+ $\mathbf{L_1}$). (A) Volume changes of MCF-7 tumors and (B) Photos of resected tumors from mice.

Thirdly, DNA cleavage experiment and immunofluorescence assay were conducted, in which phosphorylated histone 2AX (γH2AX) is an established marker forming foci at the site of DNA breaks and activates DNA damage response.[22] **Fig. 3B-C** shows that $\mathbf{ZnHL_1}$ at 25 μM already causes substantial cleavage of pUC19 DNA from its SC (supercoiled) to the NC (nicked circular) form, while both the in-cell synthesized and pre-prepared $\mathbf{ZnHL_1}$ (40 μM, 36 h) can induce a large amount of DNA breaks foci in living cells. However, zinc salt or $\mathbf{L_1}$ alone (100 μM) does not damage DNA at all. These results demonstrate that in-cell formation of $\mathbf{ZnHL_1}$ can effectively induce DNA damage response and trigger cancer cell apoptosis.

Finally, the anti-tumor efficacy was evaluated in the nude mice bearing MCF-7 tumors. When the tumor grew to *ca.* 130 mm3, mice were intratumorally injected with PBS (control), $\mathbf{L_1}$ (2 mg/kg), $ZnCl_2$ (2 mg/kg), pre-prepared $\mathbf{ZnHL_1}$ (1 mg/kg), and ZnCl2 + $\mathbf{L_1}$ combination (1 mg/kg), where the mice was injected with $ZnCl_2$ (1 mg/kg) followed with another injection with $\mathbf{L_1}$ (1 mg/kg) 1 h later to make sure the in-cell formation of $\mathbf{ZnHL_1}$. After 14 days treatment all mice were sacrificed for tumor collection. As shown in **Fig. 4**, treatment with $\mathbf{L_1}$ alone does not affect the tumor growth at all while $ZnCl_2$ exhibits a small inhibition activity. By comparison, pre-prepared $\mathbf{ZnHL_1}$ can effectively decrease tumor volume by *ca.* 47.0% compared with the control group. When in-cell $\mathbf{ZnHL_1}$ is achieved by sequential injection procedure, the inhibition effect on the tumor growth is far greater, capable of decreasing the tumor volume by *ca.* 89.5%. Tumor tissues collected for hematoxylin and eosin (H&E) staining show obvious apoptosis characteristics, *e.g.* vascuolation and nuclear condensation in ZnH_{L1} group (Fig. S17, ESI †). Moreover, all the treated nude mice do not show obvious body weight loss (Fig. S17, ESI †). These results demonstrate that in-cell synthesized $\mathbf{ZnHL_1}$ complex has excellent in vivo anti-tumor efficacy with minimum side effect.

In summary, this study proposes a facile and cheap cancer therapeutic strategy, in which the dated Schiff base can be turned into a promising theranostic chemodrug by simply using zinc salt as an auxiliary reagent. The in-cell synthesis of such Zn Schiff base complex can be tracked in real-time via the Zn^{2+} induced green-to-blue fluorescence shift and the subsequent cytoplasm-to-nucleus translocation. Owing to the nucleus penetrating capability and DNA hydrolysis activity, in-cell synthesized Zn-Schiff base complex exhibits excellent anti-cancer activity and cancer-specificity both *in vitro* and *in vivo*. In the future work, the inorganic zinc salt can be replaced by approved nutritious zinc supplements, which is more conducive to clinical application.

View Article Online
DOI: 10.1039/C9CC03480C

This work was financially supported by the National Natural Science Foundation of China [21837006, 21572282, 21401217], 973 Program [2015CB856301], Natural Science Foundation of Guangdong Province [2017A030313041], China Postdoctoral Science Foundation [2018M643290], Fundamental Research Funds for the Central Universities.

Notes and references

§There are no conflicts to declare.

1. T. Fukada, S. Yamasaki, K. Nishida, M. Murakami, T. Hirano, *J. Bio. Inorg. Chem.*, 2011, **16**, 1123.
2. H. Beraldo, D. Gambino, *Mini Rev. Med. Chem.*, 2004, **4**, 31.
3. S. Q. Zhang, X. F. Yu, H. B. Zhang, N. Peng, Z. X. Chen, Q. Cheng, X. L. Zhang, Cheng, S. H. Zhang, Y., *Mol. Nutr. Food Res.*, 2018, **62**, e170098.
4. S. A. Rider, S. J. Davies, A. N. Jha, R. Clough, J. W. Sweetman, *J. Anim. Physiol. An. N.*, 2010, **94**, 99.
5. J. Qian, L. Wang, W.Gu, X. Liu, J. Tian, S. Yan, *Dalton Trans.*, 2011, **40**, 5617.
6. B. Elisa, G. Maddalena, L. Lorena, M. Fabrizio, M. Stefano, P. Manlio, S. Claudia, T. Paolo, T. Umberto Z. Giuseppe, *J. Am. Chem. Soc.*, 2004, **126**, 4543-4549.
7. V. T. Yilmaz, C. Icsel, F. Suyunova, M. Aygun, B. Cevatemre, E. Ulukaya, *New J. Chem.*, 2017, **41**, 8092.
8. A. K. Saini, V. Sharma, P. Mathur, M. M. Shaikh, *Sci. Rep.*, 2016, **6**, 34807.
9. G. Ilaria, B. Rosa, R. David, D. L. Joaquin, L. Joao Carlos, D. C. Antonella, R. Laura, *Inorg. Chem.*, 2013, **52**, 9245.
10. X. Tian, Q. Zhang, M. Zhang, K. Uvdal, Q. Wang, J. Chen, W. Du, B. Huang, J. Wu, Y. Tian, *Chem. Sci.*, 2017, **8**, 142.
11. C. Zhang, Z. Liu, Y. Li, W. He, X. Gao, Z. Guo, *Chem. Commun.*, 2013, **49**, 11430.
12. J. Tang, ; M. Zhang, H. Y. Yin, J. Jing, D. Xie, P. Xu, J. L. Zhang, *Chem. Comm.*, 2016, **52**, 11583.
13. J. Tang, Y. B. Cai, J. Jing, J. L. Zhang, *Chem. Sci.*, 2015, **6**, 2389.
14. K. P. Divya, S. Sreejith, P. Ashokkumar, Y. Kang, Q. Peng, S. K. Maji, Y. Tong, H. Yu, Y. Zhao, P. Ramamurthy, *Chem. Sci.*, 2014, **5**, 3469.
15. J. M. Goldberg, F. Wang, C. D. Sessler, N. W. Vogler, D. Y. Zhang, W. H. Loucks, T. Tzounopoulos, S. J. Lippard, *J. Am. Chem. Soc.*, 2018, **140**, 2020.
16. B.Daniela, J. A.Horowitz, S. J. Lippard, *J. Am. Chem. Soc.*, 2011, **133**, 4101.
17. M. Shyamal, P. Mazumdar, S. Maity, S. Samanta, G. P. Sahoo, A. Misra, *ACS. Sens.*, 2016, **1**, 739.
18. D. Xie, J. Jing, Y. B. Cai, J. Tang, J. J. Chen, J. L. Zhang, *Chem. Sci.*, 2014, **5**, 2318.
19. V. Milosavljevic, Y. Haddad, M. A. MerlosRodrigo, A. Moulick, H. Polanska, D. Hynek, Z. Heger, P. Kopel, V. Adam, *PLoS One*, 2016, **11**, e0163983.
20. E. M. Conner, J. Reglinski, W. E. Smith, I. J. Zeitlin, *Biometals,* 2017, **30**, 423.
21. U. Brand, H. Vahrenkamp, *Chem. Ber.*, 1995, **128**, 787.

22. R. Rodriguez, K. M. Miller, J. V. Forment, C. R. Bradshaw, M. Nikan, S. Britton, T. Oelschlaegel, B. Xhemalce, S. Balasubramanian, S. P. Jackson, *Nat. Chem. Biol.*, 2012, **8**, 301.

View Article Online
DOI: 10.1039/C9CC03480C